ELECTRONIC STRUCTURE OF BUCKMINSTERFULLERENE C_{60} AND ABSORPTION SPECTRA OF THE $Cu_4^{2+}@C_{60}$ AND $Ag_4^{2+}@C_{60}$ CLUSTERS

Vu Bao Ngoc[1,2], Ngo Tuan Cuong[1,2,*]

[1]Faculty of Chemistry, Hanoi National University of Education, Vietnam

[2]Center for Computational Science, Hanoi National University of Education, Vietnam

Abstract: *This work systematically examines the structural, vibrational, and electronic characteristics of buckminsterfullerene C_{60} and its metal-encapsulated derivatives, $Ag_4^{2+}@C_{60}$ and $Cu_4^{2+}@C_{60}$, employing density Functional Theory (DFT) in conjunction with Time-Dependent DFT (TD-DFT). The C_{60} molecule is most stable in the icosahedral I_h point group. Due to this high symmetry, only four vibrational modes (all T_{1u}) are infrared active, with calculated frequencies of 537, 574, 1193 and 1483 cm^{-1}. Electronic analysis indicates the lowest energy electron transitions form HOMO to LUMO as well as LUMO+1 create fifteen excited states which are 3-,3-,4- and 5-fold degeneracy, and the addition of a single electron to induces a symmetry descent from $I_h \rightarrow T \rightarrow C_i$. Subsequent optimization of the metal-doped clusters reveals structural bonding between the carbon cage and the metal atoms. While Ag_4^{2+} resides at the cage center, the Cu_4^{2+} cluster adopts an off-center position. Crucially, metal encapsulation dramatically alters the optical properties. While pure C_{60} exhibits forbidden transitions in the UV-Vis region, the doped clusters display distinct absorption bands - specifically 224, 264, and 355 nm for $Ag_4^{2+}@C_{60}$, and 250, 327, and 346 nm for $Cu_4^{2+}@C_{60}$. These spectral shifts are ascribed to the participation of the transition-metal s and d orbitals in the fullerene $\pi \rightarrow \pi^*$ electronic transitions.*

Keywords: *buckminsterfullerene C_{60}, DFT, metal-encapsulated clusters, TD-DFT*

1. INTRODUCTION

The discovery of buckminsterfullerene (C_{60}) in 1985 marked a milestone in carbon science, introducing a novel molecular form composed entirely of carbon atoms. This breakthrough has led to an extensive accumulation of experimental and theoretical studies, as well as authoritative reviews and monographs, focusing on the physicochemical properties of $C_{60,}$ its derivatives, and their multifaceted applications (Nikolaev & Plakhutin, 2010; Acquah et al.., 2017; Xu et al., 2023). Two independent scientific investigations contributed to the discovery of the C_{60} molecules (Dresselhaus, Dresselhaus & Eklund, 1996). In particular, Kroto and co-workers reported infrared spectroscopic studies of carbon clusters in astrophysical contexts, which played a crucial role in its identification (Kroto et al., 1985). Another study conducted by Smalley was about the synthesis of carbon structures by laser vaporization of carbon. The unexpected finding emerged from cluster-beam experiments employing laser vaporization of a graphite rod in a helium environment to form carbon plasmas, with the primary objective of probing the characteristics of unidentified interstellar material. Among

the carbon clusters formed, a highly stable C_{60} species was rapidly identified and proposed to adopt a spheroidal cage structure (Kroto et al., 1985). In 1989, Krätschmer, Fostiropoulos, and Huffman achieved the synthesis of C_{60} by arc evaporation of graphite electrodes in an inert atmosphere, with IR and UV spectroscopy providing definitive experimental confirmation. This achievement represented a major breakthrough in fullerene science (Krätchmer, Fostiropoulos & Huffman, 1990). The molecule was named buckminsterfullerene in reference to its resemblance to the geodesic domes of Richard Buckminster Fuller. Commonly referred to as fullerenes or buckyballs, these structures established C_{60} as the third allotrope of carbon, in addition to graphite and diamond (Kroto et al., 1985).

Buckminsterfullerene is composed of 60 carbon atoms covalently bonded in a closed-cage configuration, where each carbon atom is threefold coordinated. The carbon framework consists of a network of 12 pentagonal and 20 hexagonal rings arranged in a truncated icosahedral geometry, analogous to the pattern observed on a soccer ball. This specific arrangement of pentagons and hexagons induces curvature in the carbon lattice, resulting in a highly symmetric, spherical structure with exceptional stability. Each hexagonal ring is adjacent to three pentagons and three hexagons, promoting the overall curvature of the cage. The resulting molecule has an approximate diameter of 0.7 nanometers (Dresselhaus, Dresselhaus & Eklund, 1996; Kroto et al., 1985).

Possessing a high molecular symmetry, buckminsterfullerene exhibits exceptional thermodynamic stability, enabling it to withstand elevated temperatures and pressures without structural degradation. The conjugated carbon–carbon bonding framework facilitates extensive π-electron delocalization, which gives rise to its distinctive physicochemical properties. Under appropriate conditions, particularly upon activation by high-energy radiation such as ultraviolet light, C_{60} can participate in a variety of chemical reactions. Notably, it readily undergoes addition reactions with species including hydrogen, halogens, and free radicals. Furthermore, the surface of C_{60} can be chemically modified through functionalization, allowing for the synthesis of fullerene derivatives with tunable properties tailored for specific applications (Sundqvist, 1999; Usenko, Harper & Tanguay, 2008; Hamblin, 2018; Biglova & Mustafin, 2019; Pei & Wang, 2019; Liu et al., 2024). Endohedral fullerenes are defined by the encapsulation of a dopant which can be an atom, ion, or cluster, within the interior of the fullerene cage, commonly represented as $M@C_{60}$, where the "@" symbol indicates internal confinement. This class is distinct from exohedral fullerenes, in which atoms or functional groups are chemically attached to the external surface of the C_{60} cage and are denoted as AC_{60} (Popov, Yang & Dunsch, 2013).

Buckminsterfullerene and its functional derivatives have found widespread applications in multiple disciplines. Hydrophilic fullerene derivatives are of particular interest in medicinal chemistry as antioxidants, where they play a role in mitigating the formation of reactive oxygen species. Meanwhile, hydrophobic derivatives, notably metallofullerenes, have demonstrated promising performance

in applications related to chemical sensing and photovoltaic energy conversion. Furthermore, metallofullerenes have been reported to act as efficient catalysts in a variety of organic reactions, including cycloaddition processes and Bingel-type functionalizations (Wang et al., 1999; Yin et al., 2009; Popov, Yang & Dunsch, 2013).

One of the fundamental aspects governing the behavior of buckminsterfullerene is its electronic transition dynamics, which critically influence its electrical conductivity, photophysical response, and interactions with external fields. Despite its high molecular symmetry and well-established ground-state geometry, a comprehensive understanding of the electronic transition behavior of C_{60} remains challenging. The geometrical and electronic structures of several small silver and copper clusters including Ag_4 and Cu_4 has been elucidated by Dhiman et al. (2015), who used density functional theory (DFT) calculations to show that Ag_4 and Cu_4 clusters prefer a tetrahedral geometry inside the C_{60} cavity. Their work emphasizes that the significant charge transfer from the metal core to the carbon shell not only stabilizes the endohedral complex but also results in a narrowed HOMO-LUMO gap, which is essential for understanding the electronic transition and photophysical behavior of these clusters.

The present work addresses these issues by analyzing the molecular symmetry of C_{60} in conjunction with its electronic configuration, with the aim of rationalizing the stability of its highly symmetric structure. Furthermore, the effects of symmetry reduction arising from electronic excitation and electron addition are explored in detail. This work then investigates the absorption spectra of the $Ag_4^{2+}@C_{60}$ as well as $Cu_4^{2+}@C_{60}$ clusters.

2. METHODS OF CALCULATION

In order to study the C_{60} and C_{60}^{-} as well as the $Cu_4^{2+}@C_{60}$ and $Ag_4^{2+}@C_{60}$ clusters we use the method of density functional theory (DFT) and time – dependent density functional theory (TD-DFT) (Hohenberg & Kohn, 1964; Bauernschmitt & Ahlrichs, 1996; Casida et al., 1998) which are implemented in the Gaussian 09 software (Frisch et al., 2009). Firstly, geometries of the C_{60} in several point group has been optimized using the hybrid B3LYP functional in conjunction with LANL2DZ basis set (Hay & Wadt, 1985; Becke, 1993; Perdew, Burke & Ernzerhof, 1996; Dunning & Hay, 1997). The corresponding vibrational frequency analyses along with zero-point energy (ZPE) corrections for each structure were also performed at the same calculation level after geometry optimization to confirm the absence of imaginary frequencies as well as to ensure the accuracy of the relative energies, thereby establishing that the stationary points correspond to energy minima. The electronic excited-state properties of the most stable I_h symmetric C_{60} structure were then investigated using TD-DFT at the same level of theory. The aims of these calculations are to rationalize the most stable symmetrical structure of C_{60} and characterize its electronic structures in the ground state as well as in the excited states. Thirdly, the optimization calculation has been performed for the C_{60}^{-} anion in order to study the process of descending in molecular symmetry upon electron addition. In the next step,

the geometrical structures of the Cu_4^{2+}@C_{60} and Ag_4^{2+}@C_{60} endohedral clusters were optimized, followed by TD-DFT calculations employing the B3LYP/LANL2DZ functional and basis set. These calculations were performed to predict and interpret the electronic absorption spectra, with the results reported and discussed in the subsequent section.

3. RESULTS AND DISCUSSION

3.1. Electronic structure of C_{60} under symmetry reduction from the icosahedral point group

3.1.1. Symmetry and electronic configuration

As discussed previously, buckminsterfullerene is composed of sixty carbon atoms covalently bonded within a closed-cage structure. Each carbon atom is tetravalent, with its four valence electrons participating in chemical bonding. Three electrons undergo sp^2 hybridization to form three σ bonds, which collectively constitute the structural framework of the molecule. The remaining valence electron occupies a p orbital and contributes to the formation of a delocalized π-electron system across the carbon cage (Kroto et al., 1985).

The sixty carbon atoms are arranged into a polyhedral network consisting of twelve pentagonal and twenty hexagonal faces, characteristic of a truncated icosahedral geometry. This highly symmetric arrangement is responsible for the unique electronic and structural properties of buckminsterfullerene. The optimized geometrical structure of the C_{60} molecule is illustrated in the figure below.

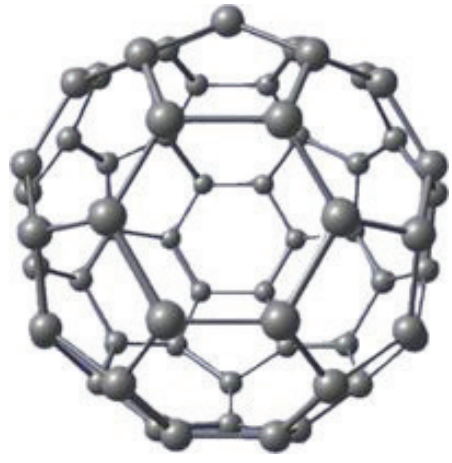

Figure 1. Optimized structure of buckminsterfullerene (C_{60})

To perform a comprehensive analysis of the C_{60} molecule, geometry optimizations were initiated using DFT calculations from input structures corresponding to a range of possible point groups, including I_h, I, T_h, T, D_{2h}, D_{5d}, D_{3d}, D_5, D_3, D_2, C_{2h}, C_{5v}, C_{3v}, C_{2v}, S_{10}, S_6, C_5, C_3, C_2, C_s, C_i. These calculations were performed to determine the optimized molecular symmetry and to evaluate the relative electronic energies associated with each point-group configuration. The resulting point groups, electronic states, and corresponding electronic energies are summarized in Table 1.

Table 1. Point groups, electronic states, and electronic energies of C_{60} optimized under different symmetry constraints

Initial Point Group	Optimized Point group	State	Total energy including ZPE correction (au)	Relative energy (eV)
I_h	I_h	^1A_g	-2285.350008	0.000
I	I_h	^1A_g	-2285.350008	0.000
T_h	I_h	^1A_g	-2285.350008	0.000
T	I_h	^1A_g	-2285.350008	0.000
D_{2h}	C_{02}	^1A	-2285.349180	0.019
D_{5d}	C_{01}	^1A	-2285.349160	0.014
D_{3d}	C_{01}	^1A	-2285.349232	0.011
D_5	C_{01}	^1A	-2285.349160	0.014
D_2	D_{02h}	^1A_g	-2285.349174	0.019
C_{5v}	C_{01}	^1A	-2285.349315	0.004
C_{3v}	C_{01}	^1A	-2285.349315	0.004
C_{2v}	D_{02h}	^1A_g	-2285.349174	0.019
S_6	C_{01}	^1A	-2285.349293	0.007
C_5	C_{01}	^1A	-2285.349248	0.010
C_3	C_{01}	^1A	-2285.349231	0.011
C_2	C_{02}	^1A	-2285.349177	0.019
C_s	C_S	$^1A'$	-2285.349301	0.006
C_i	C_I	^1A_g	-2285.349182	0.018

Based on the calculated results, the buckminsterfullerene isomer possessing icosahedral I_h symmetry is found to have the lowest total electronic energy and is therefore identified as the most stable structural form of C_{60}. The I_h point group is characterized by 120 symmetry operations, reflecting the exceptionally high symmetry of the molecule (Dresselhaus, Dresselhaus & Eklund, 1996). Within this framework, each hexagonal face is associated with a threefold rotational symmetry axis, while each pentagonal face corresponds to a fivefold rotational axis. This high degree of symmetry gives rise to the nearly spherical geometry of the molecule and underlies its well-known resemblance to

a truncated icosahedron, often described as a "soccer-ball" structure.

Structurally, the C_{60} molecule contains two distinct types of carbon–carbon bonds: thirty bonds connecting adjacent hexagonal rings and sixty bonds linking pentagonal and hexagonal rings (Kroto et al., 1985). These bonds exhibit different bond lengths, approximately 1,405 Å and 1,463Å, respectively. As a consequence of this bond-length alternation, the six-membered rings display alternating bond character, whereas the five-membered rings remain essentially bond-equalized.

Owing to its high molecular symmetry, buckminsterfullerene is also expected to exhibit a relatively simple infrared spectrum. Figure 2 display the infrared spectrum of buckminsterfullerene. In this molecule, there are 174 normal modes, however, the infrared spectrum shows only four fundamentals (at 537 cm^{-1}, 574 cm^{-1}, 1193 cm^{-1} and 1483 cm^{-1}), arising from four T_{1u} -symmetry vibrational modes, each of which is triply degenerate. This finding matches quite well with the experimental frequencies found by Krätchmer et al. (1990) (with the four most intense lines at 528, 577, 1183, 1429 cm^{-1}, respectively).

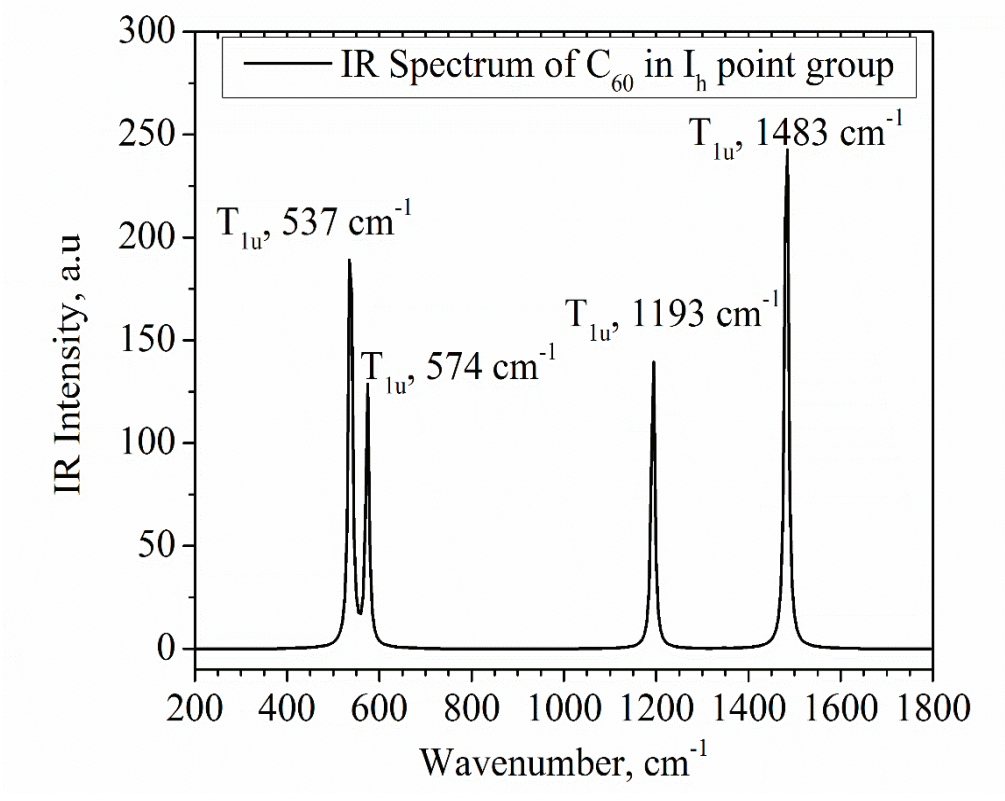

Figure 2. Infrared spectrum of buckminsterfullerene (C_{60})

The electronic configuration of buckminsterfullerene can be expressed as follows:

$\ldots H_g^2 H_g^2 H_g^2 H_g^2 H_g^2 G_g^2 G_g^2 G_g^2 G_g^2 H_u^2 H_u^2 H_u^2 H_u^2 H_u^2 \ldots$

This configuration corresponds to fourteen pairs of valence electrons occupying the outermost molecular orbitals of the C_{60} molecule. These electrons are distributed among five H_g orbitals, four G_g orbitals, and five H_u orbitals, with the latter constituting the highest occupied molecular orbital (HOMO). The calculated orbital energies for the H_g, G_g, and H_u levels are -8.027, -8.019, and -6.721 eV, respectively. The lowest unoccupied molecular orbitals (LUMOs) belong to the triply degenerate T_{1u} symmetry and are located at −3.900 eV. The resulting HOMO–LUMO energy gap is calculated to be $\Delta E = 2.820$ eV. This result is close to the B3LYP/6-311G(d,p) calculation result of 2.732 eV by Wang et al. (2012). The presence of a closed-shell, highly symmetric electronic configuration suggests that C_{60} is resistant to symmetry-lowering distortions. Consequently, the icosahedral I_h point group is confirmed as the most stable symmetry for the buckminsterfullerene molecule.

Buckminsterfullerene is classified as a non-alternant hydrocarbon due to the incorporation of five-membered rings within its carbon framework and the associated delocalization of charge. This characteristic is reflected in the asymmetric distribution of the HOMO and LUMO energy levels relative to the zero-energy reference. The molecular orbital energy spectrum further provides insight into the ionization potential and oxidation behavior of C_{60}. Notably, the calculations predict an unusually high electron affinity, indicating a strong tendency toward reduction. In particular, three molecular orbitals at −3.899 eV (T_{1u}) and three at -2.783 eV (T_{1g}) suggest that the molecule can accommodate up to twelve additional electrons under appropriate conditions. Frontier molecular orbitals of buckminsterfullerene are shown in Figure 3.

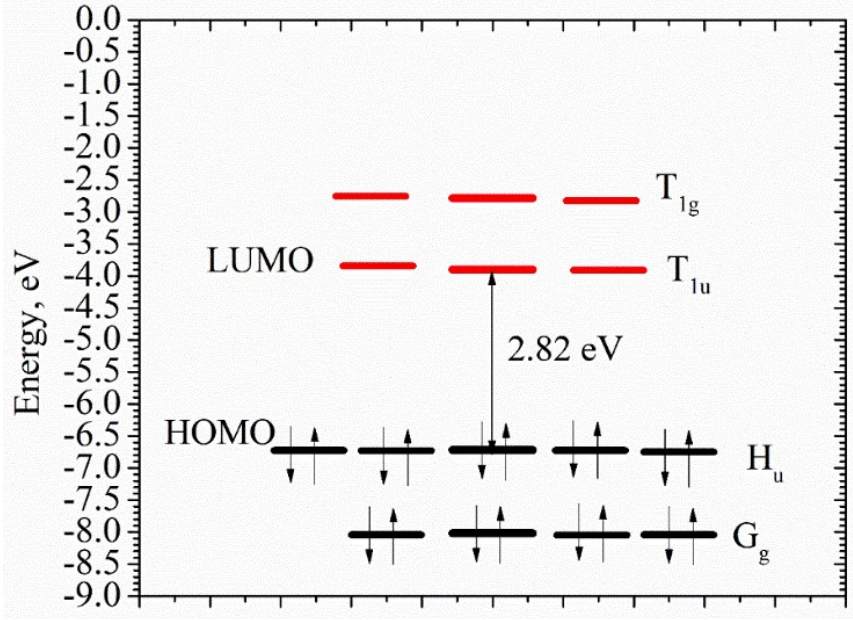

Figure 3. Frontier molecular orbitals of buckminsterfullerene (C_{60}) in the I_h point group

Figure 4 illustrates the highest occupied molecular orbital (HOMO) of H_u symmetry and the lowest unoccupied molecular orbital (LUMO) of T_{1u} (LUMO) symmetry for the molecule.

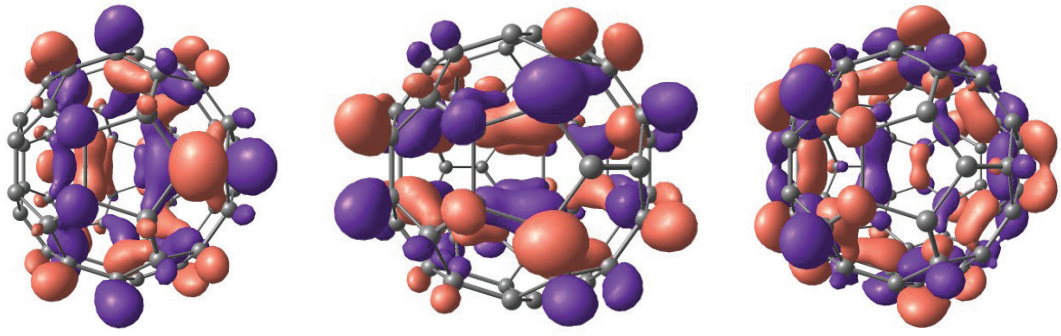

a) LUMO of C_{60} (I_h symmetry), corresponding to the triply degenerate T_{1u} alpha molecular orbitals (181–183) at −3.899 eV.

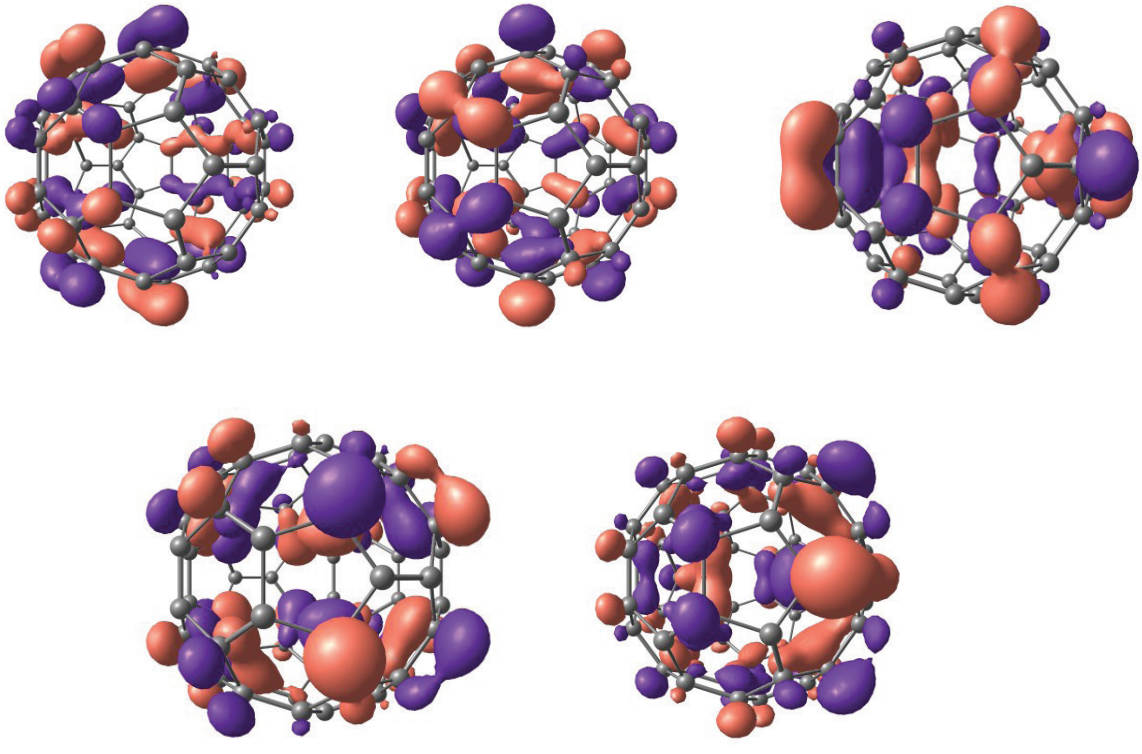

b) HOMO of C_{60} (I_h symmetry), corresponding to the fivefold-degenerate H_u alpha molecular orbitals (176–180) at −6.721 eV.

Figure 4. Frontier molecular orbitals (HOMO and LUMO) of C_{60} in the I_h point group

3.1.2. Electronic transitions in buckminsterfullerene

The two lowest-energy excited electronic configurations of buckminsterfullerene are each characterized by an approximate fifteenfold degeneracy and correspond to the following transitions:

$$(H_u)^{10}(T_{1u})^0(T_{1g})^0 \rightarrow (H_u)^9(T_{1u})^1 \text{ and } (H_u)^{10}(T_{1u})^0(T_{1g})^0 \rightarrow (H_u)^9(T_{1g})^1.$$

An electronic excitation from the H_u highest occupied molecular orbital (HOMO) to the T_{1u} lowest unoccupied molecular orbital (LUMO) results in the direct product of the H_u and T_{1u} irreducible representations, yielding a total of fifteen electronic states. According to the direct product table for the I_h point group, this product decomposes as $H_u \otimes T_{1u} = T_{1g} \oplus T_{2g} \oplus G_g \oplus H_g$. The energies of the individual electronic states arising from this transition were evaluated, and the corresponding results are summarized in Table 2.

Table 2. Electronic states generated by the HOMO (H_u) → LUMO (T_{1u}) transition in C_{60}

Excited state	Energy (eV)	Wavelength (nm)	Oscillator	S^2
T_{1g}	2.4912	497.69	0	0
T_{2g}	2.5417	487.79	0	0
G_g	2.5776	481.01	0	0
H_g	2.8561	434.10	0	0

When an electron is promoted from the H_u highest occupied molecular orbital to the T_{1g} orbital (corresponding to LUMO+1), a total of thirty electronic states is generated. This excitation is described by the direct product of the H_u and T_{1g} irreducible representations. According to the direct product table of the I_h point group, the resulting decomposition is given by $H_u \otimes T_{1g} = T_{1u} \oplus T_{2u} \oplus G_u \oplus H_u$. The energies associated with each of the resulting electronic states are presented in Table 3.

Table 3. Electronic states generated by the HOMO (H_u) → LUMO+1 (T_{1g}) transition in C_{60}

Excited state	Energy (eV)	Wavelength (nm)	Oscillator	S^2
T_{1g}	2.4912	497.69	0	0
T_{2g}	2.5417	487.79	0	0
G_g	2.5776	481.01	0	0
H_g	2.8561	434.10	0	0
T_{1u}	3.4438	360.02	0	0
H_u	3.6019	344.22	0	0
G_u	3.6776	337.14	0	0
T_{2u}	4.0455	306.48	0	0

In general, vibronic intensity-borrowing interactions between electronic states in buckminsterfullerene are expected to be relatively weak. This behavior can be attributed to the highly delocalized nature of the electronic states across the carbon cage, together with the intrinsic rigidity of the fullerene framework, which limits vibronic coupling effects.

3.1.3. Symmetry of buckminsterfullerene upon single-electron reduction (C_{60}^-)

Upon acceptance of one electron into the T_{1u} lowest unoccupied molecular orbital, neutral buckminsterfullerene (C_{60}) is converted into its monoanionic form, C_{60}^-. Prior to geometry optimization, the single-point energy (SPE) of the anion is calculated to be −62210.517 eV. The electronic configuration of can be expressed as $H_g^2 H_g^2 H_g^2 H_g^2 H_g^2 G_g^2 G_g^2 G_g^2 G_g^2 H_u^2 H_u^2 H_u^2 H_u^2 H_u^2 T_{1u}^1 T_{1u}^0 T_{1u}^0$.

Upon acceptance of an additional electron, the electronic configuration of buckminsterfullerene is altered, resulting in a reduction of its molecular symmetry. Following full geometry optimization, the initial icosahedral I_h symmetry of the neutral molecule is lowered to the C_i point group for the monoanionic species. Correspondingly, the single-point energy of C_{60}^- decreases to −62210.705 eV. The energy difference between the pre- and post-optimization electronic configurations, referred to as the rearrangement energy, is calculated to be $\Delta E_{rearrangement} = 0.188$ (eV).

Geometry optimization also induces significant changes in the energies and degeneracies of the frontier molecular orbitals. In particular, orbitals 173, 174, and 175 converge to nearly identical energies (approximately −4.67 eV), suggesting a threefold degeneracy characteristic of a T-type representation. Orbitals 176 and 177 exhibit closely spaced energy levels (−3.49 and −3.46 eV, respectively), indicating a twofold degeneracy consistent with an E-type representation. Orbital 178, located at approximately −3.39 eV, corresponds to a non-degenerate A-type representation. Additionally, orbitals 179 and 180 share nearly identical energies (around −3.30 eV), forming another doubly degenerate set. The highest occupied molecular orbital, orbital 181, is singly occupied and lies at an energy of −1.51 eV. Figure 5 shows the molecular orbital energy diagram of the buckminsterfullerene anion.

As the molecular symmetry is reduced from I_h to T and ultimately to C_i, the irreducible representations undergo corresponding splitting, with the T representation decomposing into three A representations and the E representation splitting into two A representations. Overall, the evolution of the electronic configuration of C_{60}^- upon symmetry lowering can be summarized by the following sequence:

$$(\ldots)\ H_u^2 H_u^2 H_u^2 H_u^2 H_u^2 T_{1u}^1 T_{1u}^0 T_{1u}^0 \rightarrow (\ldots)\ E_u^2 E_u^2 A_u^2 E_u^2 E_u^2 A_u^1 \rightarrow (\ldots)\ A_u^2 A_u^2 A_u^2 A_u^2 A_u^2 A_u^1$$

Based on the computational results, the buckminsterfullerene monoanion undergoes a symmetry-lowering process from the icosahedral point group I_h to C_i. Since I_h possesses several subgroup families—including tetrahedral (T), pentagonal (D_{5d}), trigonal (D_{3d}), and orthorhombic (D_2) subgroups—multiple symmetry descent pathways are theoretically possible. Accordingly, five plausible symmetry-lowering routes can be proposed: $I_h \rightarrow T \rightarrow D_2 \rightarrow C_i$, $I_h \rightarrow T \rightarrow C_2 \rightarrow C_i$, $I_h \rightarrow D_{2h} \rightarrow C_i$, $I_h \rightarrow D_{5h} \rightarrow D_5 \rightarrow C_2 \rightarrow C_i$, and $I_h \rightarrow D_{3d} \rightarrow C_2 \rightarrow C_i$.

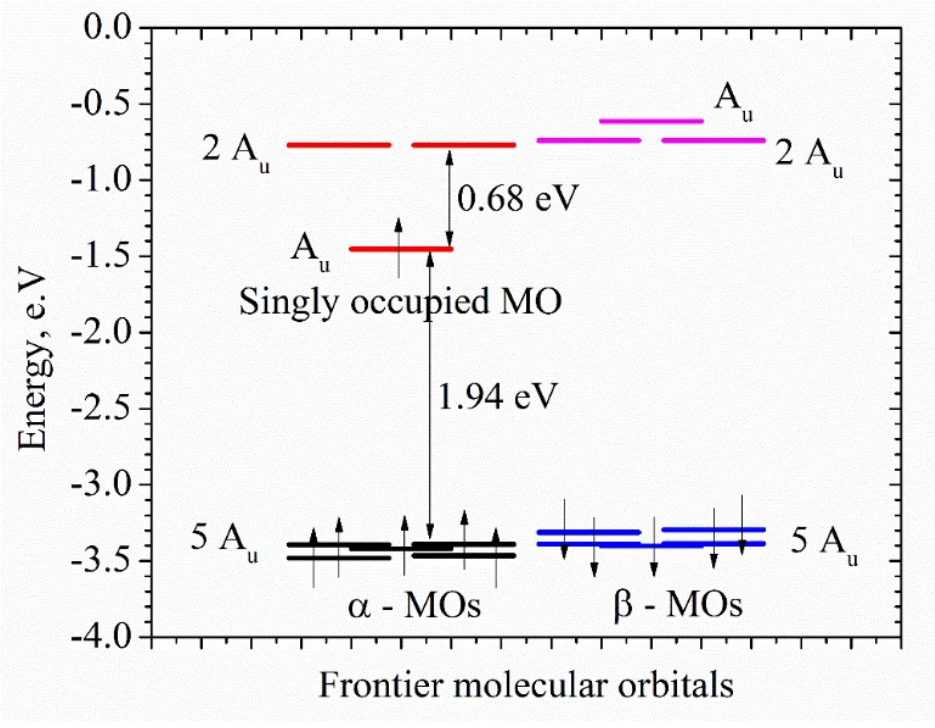

Figure 5. Molecular orbital energy diagram of the C_{60}^{-} anion in the C_i point group

After examining all possible symmetry-lowering pathways, the final optimized symmetry of the C_{60}^{-} anion is found to be C_1. The single-point energy of the isomer is −62210.705 eV, which is higher than that of the fully symmetry-broken C_1 isomer (−62210.688 eV). This energy difference indicates that the C_i structure does not correspond to the lowest-energy configuration and therefore cannot be regarded as the terminal symmetry state of the anion. Consequently, the symmetry descent pathway of buckminsterfullerene upon one-electron reduction can be summarized as: $I_h \rightarrow T \rightarrow C_i \rightarrow C_1$. Analysis of the molecular orbital energies of the optimized C_{60}^{-} anion reveals that orbitals 182 and 183, which are unoccupied, possess identical energies of approximately −0.685 eV and thus form a doubly degenerate level. The singly occupied molecular orbital (SOMO), orbital 181, lies at −1.51 eV. Orbitals 179 and 180 are nearly degenerate at around −3.30 eV and may therefore be treated as a doubly degenerate pair. Similarly, orbitals 177 and 178, with energies close to −3.42 eV, also exhibit near-degeneracy. Based on this energy pattern, the electronic configuration of the C_{60}^{-} anion can be expressed as: $[(\ldots) E_u^2 E_u^2 E_u^2 E_u^2 A_u^1 E_u^0 E_u^0]$.

Figure 6 illustrates the highest occupied molecular orbital, lowest unoccupied molecular orbital, and the frontier molecular orbitals of the C_{60}^{-} anion following full geometric optimization.

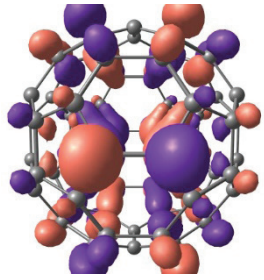

MO 182 - LUMO of C_{60}^- in C_1 point group (Unoccupied, E= -0,685 eV)

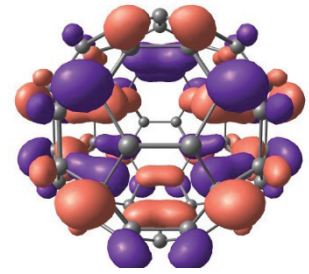

MO 183 – LUMO+1 of C_{60}^- in C_1 point group (Unoccupied, E=-0,684 eV)

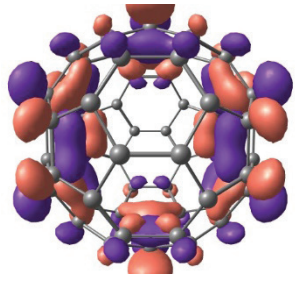

MO 181 - HOMO of C_{60}^- in C_1 point group. (Occupied, E= -1.509 eV)

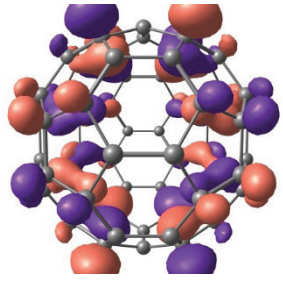

MO 179 (Occupied, E= -3.304 eV)

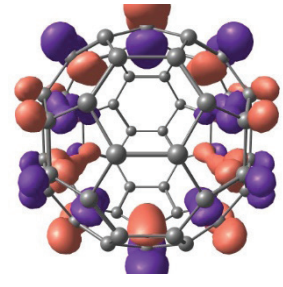

MO 180 (Occupied, E= -3.312 eV)

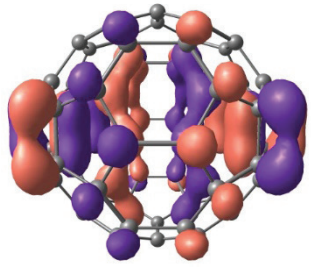

MO 178 (Occupied, E= -3.392 eV)

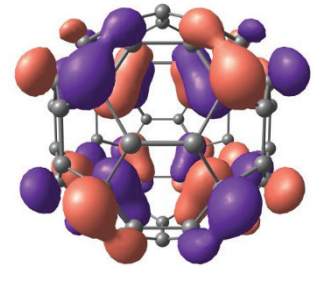

MO 177 (Occupied, E= -3.438 eV)

Figure 6. Frontier α molecular orbitals of the C_{60}^- anion in the C_1 point group

3.2. Geometrical and electronic structures and electronic transitions of $M_4^{2+}@C_{60}$

The computational results presented in Section 3.1 provide important insights into the electronic structure and symmetry behavior of the pristine C_{60} molecule. To further extend this investigation to endohedral fullerene systems, additional calculations were performed on $Cu_4^{2+}@C_{60}$ and $Ag_4^{2+}@C_{60}$ clusters, in which a tetrahedrally arranged M_4^{2+} metal cluster is encapsulated within the fullerene cage.

3.2.1. Geometrical structures of $M_4^{2+}@C_{60}$

The geometries of both endohedral clusters were fully optimized using the Gaussian 09 software package. The optimized structures provide detailed information regarding the spatial positioning of the encapsulated M_4^{2+} clusters, their interactions with the surrounding carbon cage, and the intermetallic distances within the tetrahedral metal framework.

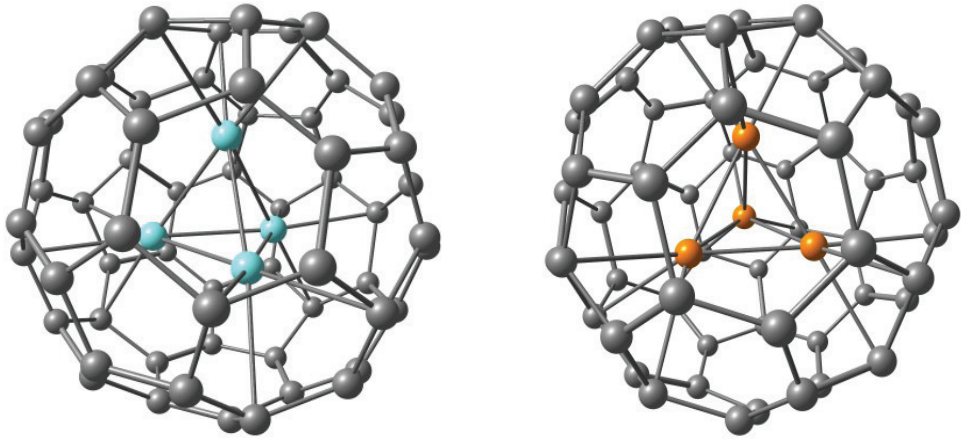

Figure 7. Geometric structure of $Ag_4^{2+}@C_{60}$ (left) and $Cu_4^{2+}@C_{60}$ (right)

For the $Ag_4^{2+}@C_{60}$ endohedral complex, the optimized structural parameters indicate that:

(i) the C–C bond lengths of the fullerene cage are slightly elongated relative to those of pristine C_{60}, with average values of approximately 1.42 Å for bonds shared by two six-membered rings and 1.48 Å for bonds connecting five- and six-membered rings.

(ii) The distances between each Ag atom and the carbon atoms belonging to both five- and six-membered rings are nearly uniform, ranging from 2.37 to 2.38 Å. When compared with the sum of the van der Waals radii of Ag (2.53 Å) and C (1.70 Å) (Bondi, 1964; Alvarez, 2013), which is about 4.23 Å, as well as with the sum of their covalent radii (Ag: 1.28 Å; C: 0.75 Å) (Pyykkö & Atsumi, 2009), equal to 2.03 Å, these Ag–C separations suggest that the Ag atoms form covalent interactions with the carbon atoms of the C_{60} cage to a certain extent.

(iii) The Ag–Ag bond lengths within the encapsulated cluster are approximately 2.46 Å, which are slightly shorter than the nearest-neighbor Ag–Ag distance in crystalline silver (≈ 2.89 Å) (Bayler et al., 1996). This contraction can be attributed

to the spatial confinement imposed by the rigid C_{60} cage, while the Ag–C covalent interactions are not sufficiently strong to significantly increase the Ag–Ag separations.

Applying the same analysis to the $Cu_4^{2+}@C_{60}$ system shows that:

(i) the C–C bond lengths within the six-membered rings are about 1.41 Å, while those between five- and six-membered rings are approximately 1.47 Å, indicating only minimal elongation relative to pristine C_{60}.

(ii) The Cu–C distances vary more significantly than in the silver analogue, ranging from 2.31 to 2.38 Å depending on the relative positions of the Cu and C atoms. When compared with the sum of the covalent radii of Cu (1.12 Å for a single bond) and C (0.75 Å) (Pyykkö & Atsumi, 2009), totaling 1.87 Å, these distances support the formation of covalent Cu–C interactions within the fullerene cage.

(iii) The Cu–Cu bond lengths inside the encapsulated cluster are approximately 2.32 Å, which are shorter than the Cu–Cu distance in crystalline copper (≈ 2.56 Å).

To further analyze the electronic characteristics of both endohedral complexes, natural bond orbital (NBO) charge calculations were performed for the Ag, Cu, and C atoms. The resulting charge distributions are summarized in Table 4.

Table 4. Charge distribution of $Cu_4^{2+}@C_{60}$ and $Ag_4^{2+}@C_{60}$

Charge (*e*)	Ag_4	Cu_4	C_{60}
$Ag_4^{2+}@C_{60}$	≈ 0.259 x 4 = 1.036		≈ 0.964
$Cu_4^{2+}@C_{60}$		≈ 0.273 x 4 = 1.092	≈ 0.908

In both endohedral complexes, the encapsulated metal cluster (Ag_4 or Cu_4) as well as the fullerene cage carry positive charges. For the $Ag_4^{2+}@C_{60}$ system, the Ag_4 cluster bears an overall positive charge of approximately +1.036 e, corresponding to an average charge of about +0.259 e on each Ag atom. The C_{60} cage carries a positive charge of approximately +0.964 e, indicating a net loss of electron density from the fullerene framework during the formation of the $Ag_4^{2+}@C_{60}$ complex.

A similar charge distribution is observed for the $Cu_4^{2+}@C_{60}$ complex. In this case, the Cu4 cluster possesses a total positive charge of approximately +1.092 e, with an average charge of about +0.273 e per Cu atom, while the C_{60} cage carries a positive charge of approximately +0.908 e. This again suggests electron density depletion from the fullerene cage upon encapsulation of the Cu_4 cluster.

A comparison between the two endohedral systems reveals that, although they share several common characteristics, distinct differences are also present. First, the spatial positions of the metal clusters within the C_{60} cage differ significantly. In $Ag_4^{2+}@C_{60}$, the nearly identical distances between each Ag atom and the two types of carbon atoms imply that the Ag_4 cluster is located close to the center of the fullerene

cage. In contrast, the Cu_4 cluster in $Cu_4^{2+}@C_{60}$ is markedly displaced from the cage center, as evidenced by the pronounced variations in Cu–C bond lengths.

Second, the incorporation of either metal cluster leads to a slight elongation of the C–C bonds in the C_{60} framework. However, the extent of this structural perturbation is smaller in $Cu_4^{2+}@C_{60}$ than in $Ag_4^{2+}@C_{60}$. This difference can be rationalized by the smaller atomic radius of Cu compared to Ag, as well as by the stronger interaction between the Ag_4 cluster and the C_{60} cage relative to that between Cu_4 and C_{60}.

3.2.2. Electronic transition of $M_4^{2+}@C_{60}$

As a consequence of bond formation between the encapsulated Ag_4^{2+} and Cu_4^{2+} clusters and the fullerene framework, the electronic structures of $Ag_4^{2+}@C_{60}$ and $Cu_4^{2+}@C_{60}$ differ markedly from that of pristine C_{60}. To investigate their excited-state properties, time-dependent density functional theory (TD-DFT) calculations were performed for the first 300 singlet excited states, yielding detailed electronic excitation information for these endohedral systems. The incorporation of the silver cluster, in particular, gives rise to numerous electronic transitions that are absent in the isolated C_{60} molecule.

The calculated results indicate that:

(i) in the low-energy region (below 2.5 eV), the electronic transitions exhibit negligible oscillator strengths, suggesting that these excitations are either symmetry-forbidden or correspond to weak charge-transfer processes between the Ag_4^{2+} or Cu_4^{2+} clusters and the C_{60} cage.

(ii) At higher excitation energies, transitions with appreciable oscillator strengths begin to emerge. These transitions can be mainly attributed to $\pi \rightarrow \pi^*$ excitations within the C_{60} framework, albeit significantly perturbed by the presence of the encapsulated Ag_4^{2+} and Cu_4^{2+} clusters. Compared with pristine C_{60}, the inclusion of transition-metal clusters induces noticeable shifts and splittings of several characteristic absorption bands, reflecting substantial electronic interactions between the metal clusters and the delocalized π-electron system of the fullerene cage.

Based on the TD-DFT results, the absorption spectra of $Ag_4^{2+}@C_{60}$ and $Cu_4^{2+}@C_{60}$ were constructed. In addition, the molecular orbitals that predominantly contribute to the electronic transitions associated with the main absorption bands were analyzed. These results are presented in Figures 8–15.

a. Absorption spectrum of $Ag_4^{2+}@C_{60}$

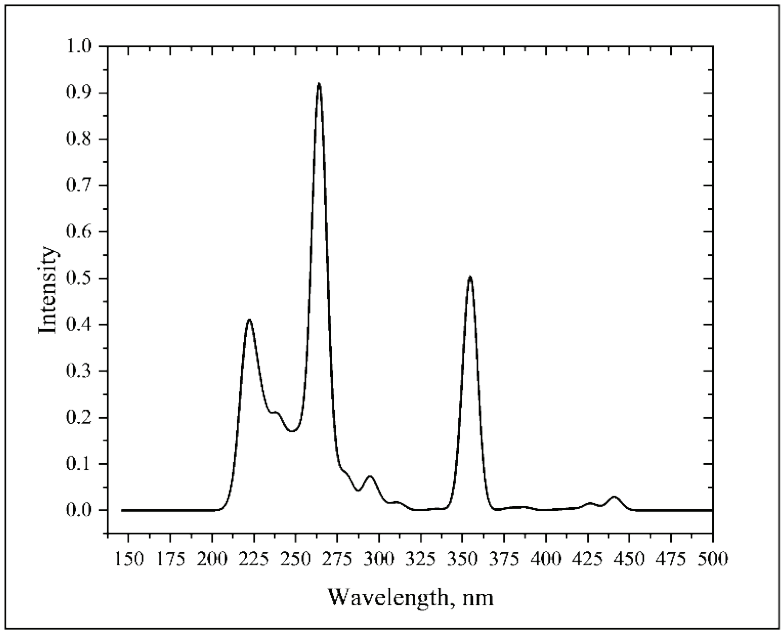

Figure 8. Absorption spectrum of $Ag_4^{2+}@C_{60}$ cluster

The calculated absorption spectrum exhibits three bands with markedly higher intensities than the remaining transitions. By correlating these spectral features with the natural bond orbital (NBO) analysis, the following observations can be made:

i) The first intense absorption band, centered at approximately 224 nm

This band mainly arises from three singlet excited states, namely S_{250}, S_{251}, and S_{252}, among the 300 calculated singlet excited states. These states are excited by ultraviolet radiation with wavelengths around 222 nm (corresponding to an excitation energy of 5.59 eV) and display relatively large oscillator strengths, with f values reaching approximately 0.42. The associated $\langle S^2 \rangle$ values are equal to zero, indicating that no spin contamination or splitting occurs and that all three states are purely singlet in character.

The electronic transition from the ground state S_0 to S_{250} is composed of several orbital excitations, including transitions from MOs 192, 205, 206, 207, and 208 to MOs 219, 228, 229, 230, and 231. Among these contributions, the excitation from MO 207 to MO 230 is dominant, with a coefficient of 0.36.

For the $S_0 \rightarrow S_{251}$ transition, electron excitations involve MOs 189, 191, 204, 205, 206, 207, and 208 to MOs 218, 219, and 227–231. In this case, the transition from MO 204 to MO 230 provides the largest contribution, corresponding to an oscillator strength of approximately f = 0.25.

The $S_0 \rightarrow S_{252}$ excitation consists of transitions from MO 193 to MO 220, from MO 198 to MO 222, and from MOs 204–208 to MOs 228–231. Among these, the transition from MO 206 to MO 229 is the most significant, with an oscillator strength of f = 0.27.

When combined with the NBO analysis, these transitions can be identified

predominantly as π → π* excitations localized on the C_{60} framework, with noticeable participation of the Ag s and d orbitals, reflecting the influence of the encapsulated silver cluster on the electronic excitation process.

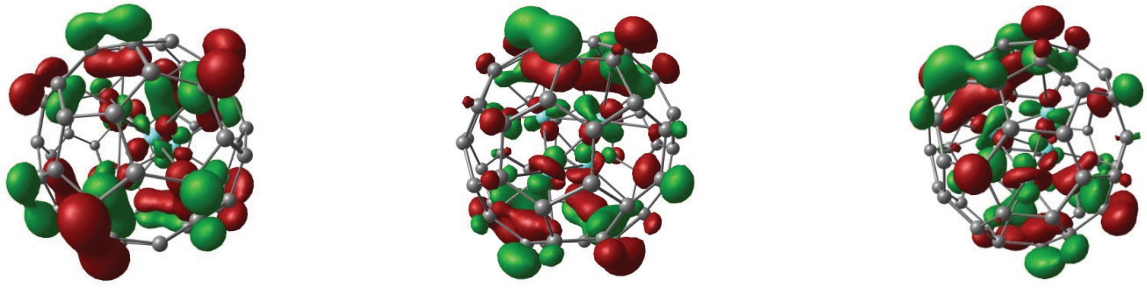

a. MO 204 (E=-0.515 eV) *b. MO 206 (E=-0.515 eV)* *c. MO 207(E=-0.515 eV)*

d. MO 229 (E=-0.290 eV) *e. MO 230 (E=-0.290 eV)*

Figure 9. Molecular orbitals that significantly involve in electronic transitions from S_o to S_{210}, S_{251}, S_{252}

ii) The second absorption band at approximately 264 nm

The second prominent band, located at around 264 nm in the ultraviolet region, is the most intense among the three major absorption features, exhibiting an oscillator strength of approximately f = 0.92. This band corresponds predominantly to π → π* electronic excitations of the system and arises from several closely spaced excited states, most notably the transitions $S_0 \rightarrow S_{137}$, $S_0 \rightarrow S_{138}$, and $S_0 \rightarrow S_{139}$.

For the excited state S_{137}, the electronic configuration involves transitions from orbitals 197, 198, and 199 to orbitals 218, 219, and 220, as well as from orbitals 213–217 to orbitals 226–230. Within this state, the excitation from MO 215 to MO 227 provides the largest contribution, with a configuration interaction coefficient of approximately 0.26.

The excited state S_{138} is similarly composed of multiple orbital transitions, including excitations from orbitals 197, 198, 199, and 213–216 to orbitals 218–220, together with transitions from orbitals 224–231. In this case, the dominant contribution arises from the transition between MO 214 and MO 227, with a coefficient of about 0.25.

The S_{139} excited state also consists of several electronic transitions, namely

from orbitals 197 and 198 to MO 218, from orbitals 198 and 199 to MO 220, and from orbitals 213–216 to orbitals 225–231. Among these contributions, the excitation from MO 213 to MO 228 exhibits the highest configuration coefficient, approximately equal to 0.25.

Analysis based on the NBO calculations indicates that the occupied orbitals involved in these transitions are composed of mixed Ag s and d orbitals together with C p orbitals, whereas the corresponding virtual orbitals are predominantly formed by the p orbitals of carbon atoms. This observation confirms that the intense absorption at ~264 nm arises from π → π* transitions of the fullerene cage, significantly perturbed by orbital hybridization with the encapsulated silver cluster.

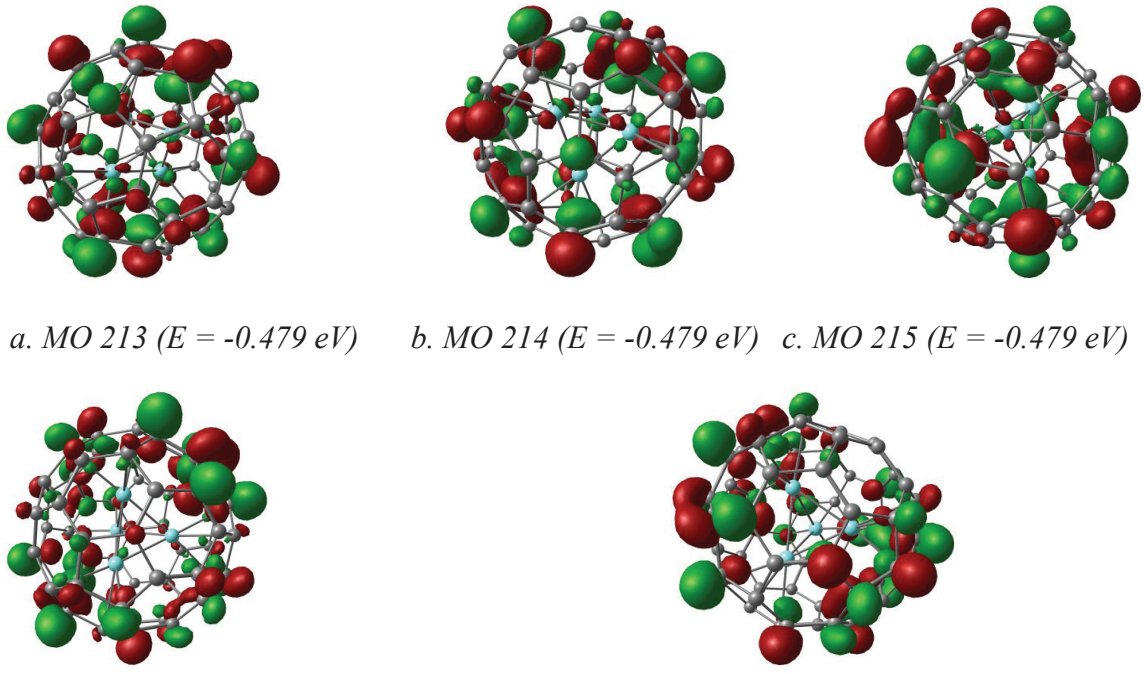

a. MO 213 (E = -0.479 eV) *b. MO 214 (E = -0.479 eV)* *c. MO 215 (E = -0.479 eV)*

d. MO 227 (E = -0.293 eV) *e. MO 228 (E = -0.293 eV)*

Figure 10. Molecular orbitals that significantly involve in electronic transitions from S_o to S_{137}, S_{138}, S_{139}

iii) The third absorption band at approximately 355 nm

The third major absorption feature appears at around 355 nm in the ultraviolet region and exhibits moderate intensity, with an oscillator strength of approximately f = 0.5. This band originates from several closely spaced singlet excited states, primarily the transitions $S_0 \rightarrow S_{55}$, $S_0 \rightarrow S_{56}$, and $S_0 \rightarrow S_{57}$. The corresponding $\langle S^2 \rangle$ values are equal to zero, confirming that all these excited states are pure singlets.

These excitations mainly involve electron transitions from occupied orbitals 203–207 and 213–217 to virtual orbitals 218–223. In the S_{55} excited state, multiple electronic transitions contribute to the absorption band; however, the transition from MO 203

to MO 220 provides the largest contribution, with a configuration interaction coefficient of approximately 0.31.

For the S_{56} excited state, the excitation from MO 203 to MO 219 exhibits the highest oscillator strength ($f \approx 0.32$), making it the dominant contribution to this absorption feature. In the case of S_{57}, the most significant contribution arises from the transition between MO 203 and MO 218, which has a notably large configuration coefficient of 0.59.

Based on the NBO analysis, these excitations can be assigned predominantly to $\pi \rightarrow \pi^*$ transitions within the C_{60} framework, with additional involvement of the Ag s and d orbitals, indicating hybridization effects induced by the encapsulated silver cluster.

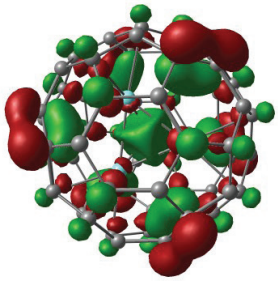

a. MO 203 (E = -0.527 eV)

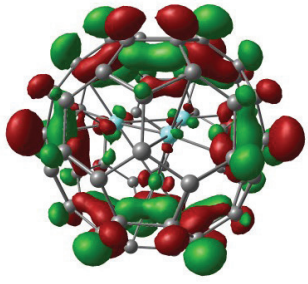

b. MO 218 (E = -0.376 eV)

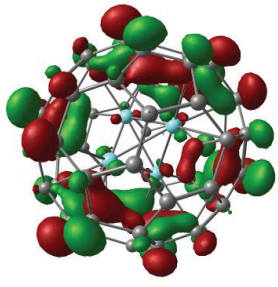

c. MO 219 (E = -0.376 eV)

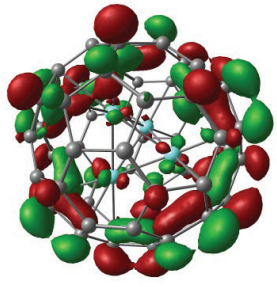

d. MO 220 (E = -0.376 eV)

Figure 11. Molecular orbitals significantly involved in the electronic transitions from S_0 to S_{55}, S_{56}, and S_{57}

iv) Other weaker absorption bands

In addition to the three main absorption bands discussed above, the calculated spectrum also displays several weaker features, such as bands located around 300 nm and near 440 nm. These bands are characterized by very low intensities, reflecting the small oscillator strengths associated with the corresponding excited states. For excited states with oscillator strengths equal to zero, no absorption peaks are observed in the calculated spectrum; this is the case for the lowest-lying excited states, such as the first twenty singlet excited states. The absence of these transitions in the absorption spectrum can be attributed to orbital selection rules, which render these electronic excitations symmetry-forbidden.

b. Absorption spectrum of $Cu_4^{2+}@C_{60}$

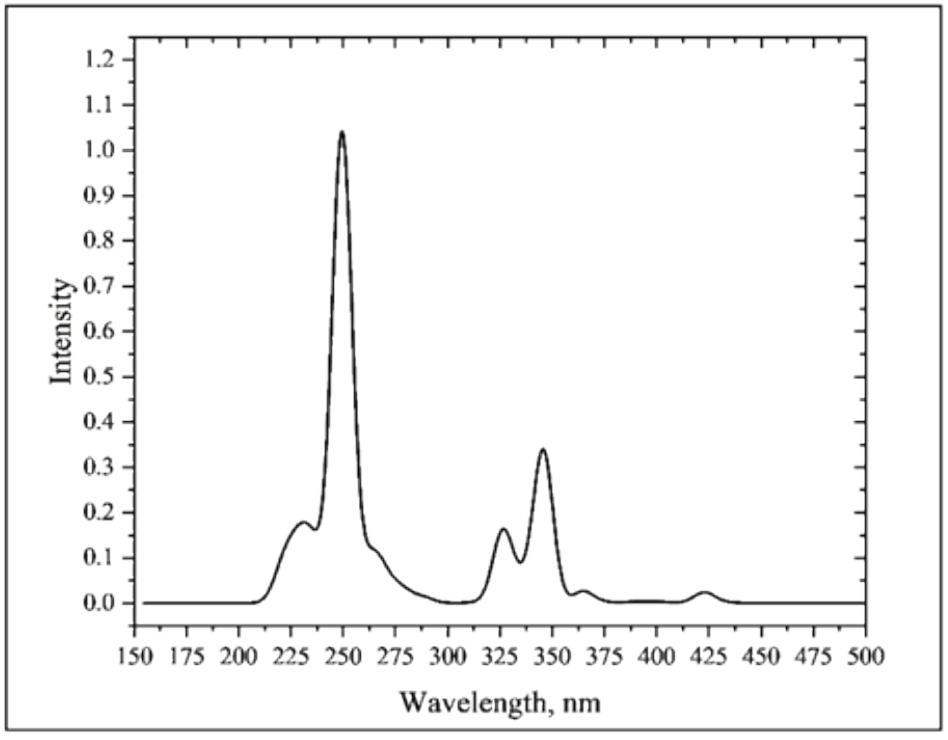

Figure 12. Absorption spectrum of $Cu_4^{2+}@C_{60}$

The absorption spectrum obtained from the TD-DFT calculations exhibits several pronounced bands. Among them, three bands located at approximately 250, 327, and 346 nm were selected for detailed analysis, as they display significantly higher intensities than the remaining features. All excited states involved in these transitions possess $\langle S^2 \rangle$ values equal to zero, confirming their pure singlet character and the absence of spin splitting.

i) The absorption band centered at approximately 250 nm

This band is the most intense feature in the spectrum, with an oscillator strength of about f = 1.04. It mainly originates from three closely spaced excited states, namely $S_0 \rightarrow S_{200}$, $S_0 \rightarrow S_{201}$, and $S_0 \rightarrow S_{202}$. In these excited states, the electronic excitations predominantly involve transitions from doubly occupied orbitals 189–191 and 213–216 to virtual orbitals 219, 220, and 229–231.

For the excited state S_{200} the transition from MO 213 to MO 231 provides the largest contribution, with a configuration interaction coefficient of approximately 0.26. In the subsequent excited state S_{201}, the dominant excitation corresponds to the transition from MO 213 to MO 230, with a coefficient of about 0.275. In the excited state S_{202}, the most significant contribution arises from the electron transfer between MO 191 and MO 220, which exhibits a configuration coefficient of approximately 0.27.

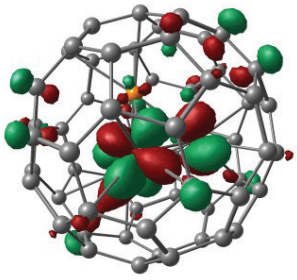

a. MO 191 (E = -0.576 eV)

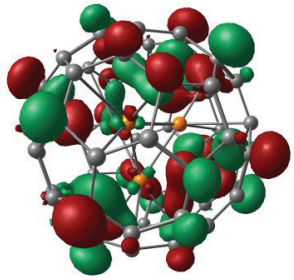

b. MO 213 (E = -0.479 eV)

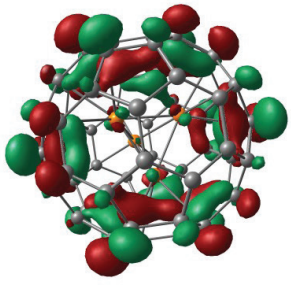

c. MO 220 (E = -0.375 eV)

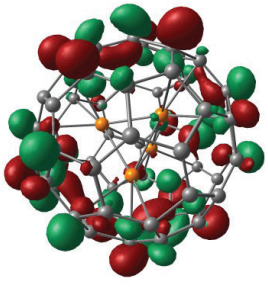

d. MO 230 (E = -0.287 eV)

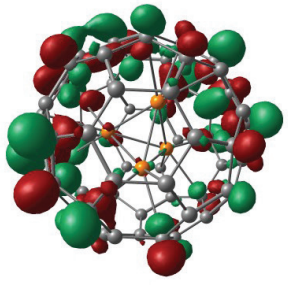

e. MO 231 (E = -0.287 eV)

Figure 13. Molecular orbitals significantly involved in the electronic transitions from S_o to S_{200}, S_{201}, S_{202}

ii) The absorption band at approximately 327 nm

The absorption feature centered at around 327 nm exhibits relatively low intensity, with an oscillator strength of approximately f ≈ 0.16. This band originates from three closely spaced excited states, namely S_{67}, S_{68}, and S_{69}. The electronic transitions contributing to these excited states primarily involve excitations from occupied orbitals 200–203 to virtual orbitals 218–220.

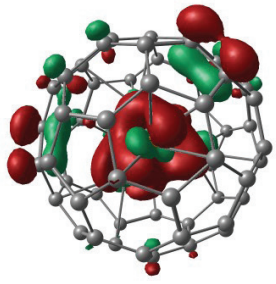

a. MO 200 (E = -0.539 eV)

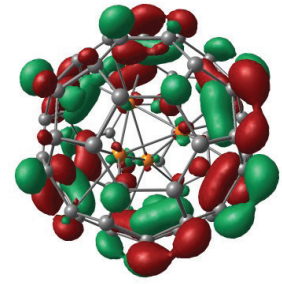

b. MO 218 (E =-0.375 eV)

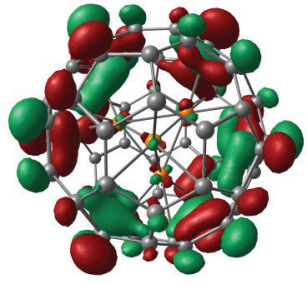

c. MO 219 (E = -0.375 eV)

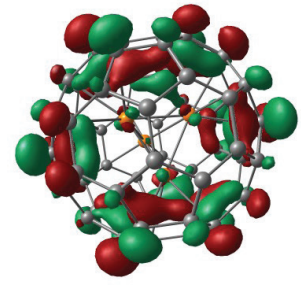

d. MO 220 (E =-0.375 eV)

Figure 14. Molecular orbitals significantly involved in the electronic transitions $S_o \rightarrow S_{67,} S_0 \rightarrow S_{68}$, $S_0 \rightarrow S_{69}$

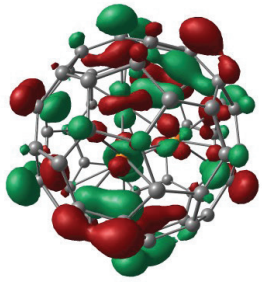

a. MO 207 (E = -0.519 eV)

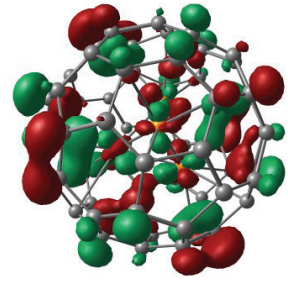

b. MO 208 (E = -0.518 eV)

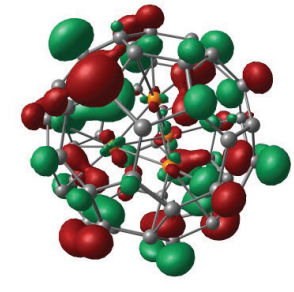

c. MO 214 (E = -0.479 eV)

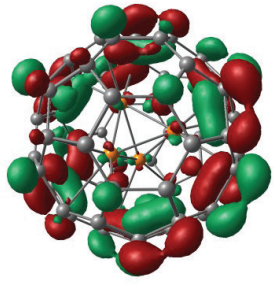

d. MO 218 (E = -0.375 eV)

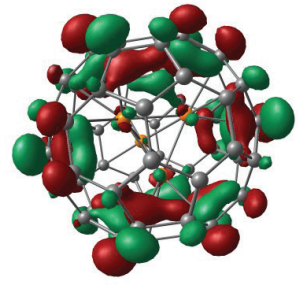

e. MO 220 (E = -0.375 eV)

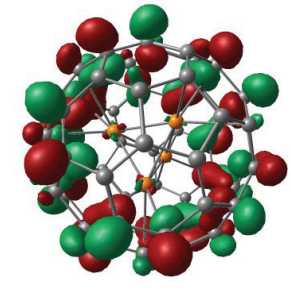

f. MO 221 (E = -0.336 eV)

Figure 15. Molecular orbitals significantly involved in the electronic transitions $S_0 \rightarrow S_{55}$, $S_0 \rightarrow S_{56}$, $S_0 \rightarrow S_{57}$

iii) The absorption band centered at approximately 346 nm

The final prominent absorption band appears at around 346 nm with a moderate oscillator strength of f ≈ 0.34. This band originates from three excited states, namely $S_0 \rightarrow S_{55}$, $S_0 \rightarrow S_{56}$, and $S_0 \rightarrow S_{57}$. These excited states are formed through multiple electronic transitions, mainly involving excitations from occupied orbitals 201–209 and 213–217 to virtual orbitals 218–223.

For the excited state S_{55}, a total of 17 individual electronic transitions were identified between the corresponding initial and final orbitals. However, all of these transitions exhibit relatively small configuration interaction coefficients, with none exceeding 0.20. In the case of excited state S_{56}, the transition from MO 208 to MO 218 provides the dominant contribution, characterized by a combination coefficient of approximately 0.23. Similarly, although excited state S_{57} comprises numerous electronic transitions, the excitation from orbital 207 to orbital 220 represents the most significant contribution, with a combination coefficient of about 0.22.

iv) Other weaker absorption bands

The calculated absorption spectrum also exhibits several additional bands with relatively low intensity, notably those appearing at approximately 360 nm and around 425 nm. These bands originate from excited states associated with smaller oscillator strengths. Excited states with an oscillator strength f equal to zero do not contribute to the absorption spectrum and therefore are not observed, as such electronic transitions are forbidden according to the electric dipole selection rules.

4. CONCLUSION

Based on the B3LYP/LANL2DZ density functional theory (DFT) calculations carried out in this work, buckminsterfullerene C_{60} is found to be most stable in the icosahedral (I_h) point group. Its electronic configuration can be described as … $H_g^2 H_g^2 H_g^2 H_g^2 H_g^2 G_g^2 G_g^2 G_g^2 G_g^2 H_u^2 H_u^2 H_u^2 H_u^2 H_u^2 T_{1u}^0 T_{1u}^0 T_{1u}^0$… Owing to its highly symmetric structure, although C_{60} possesses more than 170 vibrational modes, only four infrared-active modes are observed, all belonging to the T_{1u} irreducible representation. The calculated IR frequencies for these modes are 537 cm^{-1}, 574 cm^{-1}, 1193 cm^{-1}, and 1483 cm^{-1}.

Time-dependent DFT (TD-DFT) calculations of the electronic absorption spectrum indicate that the two lowest electronic transitions, from the HOMO (H_u) to LUMO (T_{1u}) and to the LUMO+1 (T_{1g}), each give rise to fifteen excited states with 3-, 3-, 4-, and 5-fold degeneracies. The C_{60} molecule exhibits an exceptionally high electron affinity and thus has the capability to accept additional electrons under suitable conditions. During the one-electron reduction process, buckminsterfullerene undergoes a symmetry lowering from I_h to T and subsequently to C_i, accompanied by changes in the electronic configuration: (…) $H_u^2 H_u^2 H_u^2 H_u^2 H_u^2 T_{1u}^1 T_{1u}^0 T_{1u}^0$ *(I_h)* → (…) $E_u^2 E_u^2 A_u^2 E_u^2 E_u^2 A_u^1$ *(T)* → (…) $A_u^2 A_u^2 A_u^2 A_u^2 A_u^2 A_u^1$ *(C_i)*

Furthermore, DFT geometry optimizations and TD-DFT calculations were performed for the endohedral clusters $Ag_4^{2+}@C_{60}$ and $Cu_4^{2+}@C_{60}$. The results reveal that these two systems share similar structural characteristics; however, the Ag_4^{2+} cluster is located near the center of

the C_{60} cage, whereas the Cu_4^{2+} cluster is significantly off-center. In both cases, bonding interactions between the metal atoms and the carbon cage are formed. The encapsulation of the metal clusters leads to substantial changes in the optical absorption properties of C_{60}, transforming it from a molecule with no allowed UV–Vis absorption bands (oscillator strength equal to zero) into systems exhibiting several pronounced absorption bands. Specifically, $Ag_4^{2+}@C_{60}$ shows absorption peaks at approximately 224 nm, 264 nm, and 355 nm, while $Cu_4^{2+}@C_{60}$ exhibits bands at around 250 nm, 327 nm, and 346 nm. These spectral modifications arise from the participation of the transition-metal s and d orbitals in the $\pi \rightarrow \pi^*$ electronic transitions of the buckminsterfullerene framework.

Acknowledgement: *This article is an upgraded version of the undergraduate thesis by author Vu Bao Ngoc, defended in 2025 at Hanoi National University of Education.*

Author Information:

Vu Bao Ngoc, Faculty of Chemistry, Hanoi National University of Education - Center for Computational Science, Hanoi National University of Education, Vietnam

Email: vubaongoc04102003@gmail.com

Assoc. Prof. Dr. Ngo Tuan Cuong *(*Corresponding author),* Faculty of Chemistry, Hanoi National University of Education - Center for Computational Science, Hanoi National University of Education, Vietnam

Email: cuongnt@hnue.edu.vn

Author Contributions:

Vu Bao Ngoc: performed calculations, analyzed the data, drafted and revised the manuscript.

Ngo Tuan Cuong: conceptualized and supervised the study; reviewed, revised, edited, and finalized the manuscript.

Article Information:

Received: January 22, 2026

Revised: March 07, 2026

Accepted: March 08, 2026

Note

The authors declare no competing interests regarding this article

REFERENCES

Acquah, S. F. A., Penkova, A. V., Markelov, D. A., Semisalova, A. S., Leonhardt, B. E., & Magi, J. M. (2017). Review—The beautiful molecule: 30 years of C_{60} and its derivatives. *ECS Journal of Solid State Science and Technology*, M3155–M3162.

Alvarez, S. (2013). A cartography of the van der Waals territories. *Dalton Transactions, 42*, 8617–8636.

Bauernschmitt, R., & Ahlrichs, R. (1996). Treatment of electronic excitations within the adiabatic approximation of time-dependent density functional theory. *Chemical Physics Letters, 256*, 454–464.

Bayler, A., Schier, A., Bowmaker, G. A., & Schmidbaur, H. (1996). Gold is smaller than silver. Crystal structures of [bis(trimesitylphosphine)gold(I)] and [bis(trimesitylphosphine)silver(I)] tetrafluoroborate. *Journal of the American Chemical Society, 118*(29), 7006–7007.

Becke, A. D. (1993). Density-functional thermochemistry. III. The role of exact exchange. *Journal of Chemical Physics, 98*, 5648–5652.

Biglova, Y. N., & Mustafin, A. G. (2019). Nucleophilic cyclopropanation of [60] fullerene by the addition–elimination mechanism. *RSC Advances, 9*(39), 22428–22498.

Bondi, A. (1964). van der Waals volumes and radii. *Journal of Physical Chemistry, 68*(3), 441–451.

Casida, M. E., Jamorski, C., Casida, K. C., & Salahub, D. R. (1998). Molecular excitation energies to high-lying bound states from time-dependent density-functional response theory: Characterization and correction of the time-dependent local density approximation ionization threshold . *Journal of Chemical Physics, 108*, 4439–4449.

Dhiman, S., Kumar, R. & Dharamvir, K. (2015). DFT study of Cu and Ag clusters inside C_{60}. *Journal of Molecular Structure*, *1100*, 328–337.

Dresselhaus, M. S., Dresselhaus, G., & Eklund, P. C. (1996). *Science of fullerenes and carbon nanotubes*. Academic Press.

Dunning, T. H., Jr., & Hay, P. J. (1997). Modern theoretical chemistry. In H. F. Schaefer III (Ed.), *Modern theoretical chemistry 3*, 1–28). Plenum Press.

Frisch, M. J. et al. (2009). *Gaussian 09*. Gaussian, Inc.

Hamblin, M. R. (2018). Fullerenes as photosensitizers in photodynamic therapy: Pros and cons. *Photochemical & Photobiological Sciences, 17*(11), 1515–1533.

Hay, P. J., & Wadt, W. R. (1985). Ab initio effective core potentials for molecular calculations—Potentials for the transition-metal atoms Sc to Hg. *Journal of Chemical Physics, 82*, 270–283.

Hohenberg, P., & Kohn, W. (1964). Inhomogeneous electron gas. *Physical Review, 136*, B864–B871.

Krätchmer, W., Fostiropoulos, K., & Huffman, D. R. (1990). The infrared and ultraviolet absorption spectra of laboratory-produced carbon dust: Evidence for the presence of the C_{60} molecule. *Chemical Physics Letters, 170*, 167–170.

Kroto, H. W., Heath, J. R., O'Brien, S. C., Curl, R. F., & Smalley, R. E. (1985). C60: Buckminsterfullerene. *Nature, 318*, 162–163.

Liu, Y., Gao, Y., Altalhi, T., Liu, D.-J., & Yakobson, B. I. (2024). A quantum mechanical MP2 study of the electronic effect of nonplanarity on the carbon pyramidalization of fullerene C_{60}. *Nanomaterials, 14*(19), 1576.

Nikolaev, A. V., & Plakhutin, B. N. (2010). C_{60} fullerene as a pseudoatom of the icosahedral symmetry. *Russian Chemical Reviews, 79*, 729–755.

Pei, C., & Wang, L. (2019). Recent progress on high-pressure and high-temperature studies of fullerenes and related materials. *Matter and Radiation at Extremes, 4*(2), 028201.

Perdew, J. P., Burke, K., & Ernzerhof, M. (1996). Generalized gradient approximation made simple. *Physical Review Letters, 77*, 3865–3868.

Popov, A. A., Yang, S., & Dunsch, L. (2013). Endohedral fullerenes. *Chemical Reviews, 113*(8), 5989–6113.

Pyykkö, P., & Atsumi, M. (2009). Molecular single-bond covalent radii for elements 1–118. *Chemistry – A European Journal, 15*(1), 186–197.

Sundqvist, B. (1999). Fullerenes under high pressures. *Advances in Physics, 48*(1), 1–134.

Usenko, C. Y., Harper, S. L., & Tanguay, R. L. (2008). Fullerene C60 exposure elicits an oxidative stress response in embryonic zebrafish. *Toxicology and Applied Pharmacology, 229*(1), 44–55.

Wang, I. C., Tai, L. A., Lee, D. D., Kanakamma, P. P., Shen, C. K.-F., Luh, T.-Y., Cheng, C. H., & Hwang, K. C. (1999). C_{60} and water-soluble fullerene derivatives as antioxidants against radical-initiated lipid peroxidation. *Journal of Medicinal Chemistry, 42*(22), 4614–4620.

Wang, H., He, Y., Li, Y., & Su, H. (2012). Photophysical and Electronic Properties of Five PCBM-like C_{60} Derivatives: Spectral and Quantum Chemical View. *J. Phys. Chem. A*, *116*, 255–262.

Xu, J., Bakker, J. M., Lushchikova, O. V., Lievens, P., Janssens, E., & Hou, G.-L. (2023). Pentagon, hexagon, or bridge? Identifying the location of a single vanadium

cation on buckminsterfullerene surface. *Journal of the American Chemical Society, 145*, 22243–22251.

Yin, J.-J., Lao, F., Fu, P. P., Wamer, W. G., Zhao, Y., Wang, P. C., Qiu, Y., Sun, B., Xing, G., Dong, J., Liang, X.-J., & Chen, C. (2009). *Biomaterials, 30*(4), 611–621.

CẤU TRÚC ĐIỆN TỬ CỦA BUCKMINSTERFULLERENE C_{60} VÀ PHỔ HẤP THỤ CỦA CÁC CỤM $Cu_4^{2+}@C_{60}$ VÀ $Ag_4^{2+}@C_{60}$

Vũ Bảo Ngọc[1], Ngô Tuấn Cường[1,2,*]

[1]Khoa Hóa học, Đại học Sư phạm Hà Nội, Việt Nam

[2]Trung tâm Khoa học tính toán, Đại học Sư phạm Hà Nội, Việt Nam

Tóm tắt: *Nghiên cứu này khảo sát các tính chất cấu trúc, dao động và điện tử của buckminsterfullerene (C_{60}) cũng như các cụm kim loại lồng trong lồng carbon, bao gồm $Ag_4^{2+}@C_{60}$ và $Cu_4^{2+}@C_{60}$, sử dụng Lý thuyết phiếm hàm mật độ (DFT) với phiếm hàm/bộ hàm cơ sở B3LYP/LANL2DZ và DFT phụ thuộc thời gian (TD-DFT). Phân tử C_{60} bền vững nhất ở nhóm điểm đối xứng nhị thập diện (I_h). Do tính đối xứng cao này, chỉ có bốn mode dao động (đều thuộc biểu diễn bất khả quy T_{1u}) là hoạt động trên phổ hồng ngoại, với các tần số tính toán lần lượt là 537, 574, 1193, và 1483 cm^{-1}. Phân tích điện tử cho thấy sự chuyển mức electron từ HOMO lên LUMO hay LUMO + 1 đều tạo thành 15 trạng thái kích thích singlet bao gồm các trạng thái suy biến bậc 3, 3, 4 và 5, và việc C_{60} nhận thêm một electron dẫn đến sự giảm đối xứng từ $I_h \rightarrow T \rightarrow C_i$.*

Quá trình tối ưu hóa các cụm pha tạp kim loại sau đó cho thấy sự hình thành liên kết giữa lồng carbon và các nguyên tử kim loại. Trong khi Ag_4^{2+} nằm tại tâm lồng, cụm Cu_4^{2+} lại chiếm vị trí lệch tâm. Đáng chú ý, việc lồng kim loại làm thay đổi đáng kể các tính chất quang học của C_{60}. Trong khi C_{60} tinh khiết không có dải hấp thụ trong vùng UV-Vis (do các chuyển mức bị cấm), các cụm pha tạp hiển thị các dải hấp thụ rõ rệt - cụ thể là 224, 264 và 355 nm đối với $Ag_4^{2+}@C_{60}$, và 250, 327 và 346 nm đối với $Cu_4^{2+}@C_{60}$. Nguyên nhân của sự thay đổi này là do sự tham gia của các orbital s và d của kim loại chuyển tiếp vào các chuyển mức $\pi \rightarrow \pi^*$ của phân tử fullerene.

Từ khóa: *buckminsterfullerene C_{60}, cụm kim loại trong C_{60}, phương pháp phiếm hàm mật độ, phương pháp phiếm hàm mật độ phụ thuộc thời gian*

Thông tin tác giả:

Vũ Bảo Ngọc, Khoa Hóa học, Đại học Sư phạm Hà Nội, Việt Nam - Trung tâm Khoa học tính toán, Đại học Sư phạm Hà Nội, Việt Nam

Email: vubaongoc04102003@gmail.com

PGS. TS. Ngô Tuấn Cường *(*Tác giả liên hệ)*, Khoa Hóa học, Đại học Sư phạm Hà Nội, Việt Nam - Trung tâm Khoa học tính toán, Đại học Sư phạm Hà Nội, Việt Nam

Email: cuongnt@hnue.edu.vn

Ghi chú

Các tác giả xác nhận không có tranh chấp về lợi ích đối với bài báo này.